Selectivity Trends Between Oxygen Evolution and Chlorine Evolution on Iridium-Based Double Perovskites in Acidic Media

Johannes G. Vos,[†] Zhichao Liu,[†] Florian D. Speck,[‡] Nickson Perini,[§] Wentian Fu,[†] Serhiy Cherevko,[∥] and Marc T. M. Koper*,[†]

[†]Leiden Institute of Chemistry, Leiden University, P.O. Box 9502, 2300 RA Leiden, The Netherlands

[‡]Department of Chemical and Biological Engineering, Friedrich-Alexander-Universität Erlangen-Nürnberg, 91058 Erlangen, Germany

[§]Sao Carlos Institute of Chemistry, Sao Paulo University, Avenida Trabalhador São Carlense, 400, 13566-590, São Carlos, Sao Paulo, Brazil

[∥]Helmholtz-Institute Erlangen-Nürnberg for Renewable Energy (IEK-11), Forschungszentrum Jülich, Egerlandstrasse 3, 91058 Erlangen, Germany

S *Supporting Information*

ABSTRACT: The electrochemical chlorine evolution reaction (CER) and oxygen evolution reaction (OER) represent core processes in the production of chlorine, relevant to bulk chemical manufacturing, and water splitting, the most promising technology for renewable energy storage. Unfortunately, because of an apparent coupling between their key binding intermediates, the two reactions can easily occur simultaneously, which is never an attractive outcome. In this work, using a series of iridium-based double perovskites and rotating ring-disk voltammetry to deconvolute parallel OER and CER currents, we explored the interdependence of CER and OER in dilute acidic chloride solutions of up to 120 mM, where both reactions may occur in parallel with similar current densities. We also employed online inductively coupled plasma-mass spectrometry (ICP-MS) measurements to probe the material stability and its dependence on chloride concentration. For all studied materials, we found a strong linear correlation between CER and OER activity as well as a comparable selectivity, strengthening the suggestion that OER and CER follow a scaling relationship. It was also found that chloride selectively enhances the dissolution of the noble metal component. A reaction order analysis was performed to gain insight into the CER mechanism, the effect of surface area changes due to adventitious leaching, and the observed suppressing effect of chloride on OER.

KEYWORDS: chlorine evolution, oxygen evolution, selectivity, electrocatalysis, electrochemical mass spectrometry, iridium dissolution, rotating ring-disk electrode
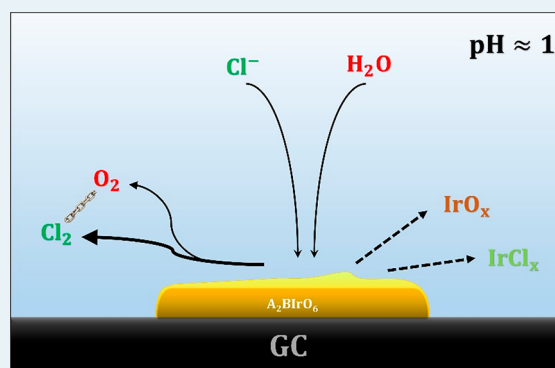
1. INTRODUCTION

The electrochemical chlorine evolution reaction (CER) and oxygen evolution reaction (OER) both lie at the heart of large scale electricity-to-chemical conversion steps, making them highly important with regard to a renewable-based energy infrastructure.[1−5] During chlorine evolution, chloride ions are oxidized to chlorine gas (Cl_2). Likewise, oxygen evolution involves the oxidation of water into O_2, along with the release of protons. The reactions proceed via

$$2H_2O \rightarrow O_2 + 4H^+ + 4e^- \qquad (1)$$

$$E^\circ_{O_2/H_2O} = 1.229 \text{ V vs RHE}$$

$$2Cl^- \rightarrow Cl_2 + 2e^- \qquad (2)$$

$$E^\circ_{Cl_2/Cl^-} = (1.358 + 0.059 \text{ pH}) \text{ V vs RHE}$$

Note that the equilibrium potential for the OER is pH-dependent on the normal hydrogen electrode (NHE) scale and therefore pH-independent of the reversible hydrogen electrode (RHE) scale, whereas the reverse is true for CER.

CER is the core reaction in the chlor-alkali process and allows the production of chlorine and caustic soda, bulk chemicals that are required in large amounts throughout the chemical industry.[6,7] The two-electron nature of the reaction means it exhibits very fast kinetics,[8] but due to its relatively high equilibrium potential, the chlor-alkali process is very energy intensive. The required power input to drive chlorine evolution is the most significant economic (and environmental) cost.[9−12] A substantial body of research has thus gone in studying

optimum process conditions for CER, since the large scale of the process means that even small efficiency gains can have a large impact.[13−15]

OER represents the desired anodic reaction in water electrolysis, since O_2 is environmentally harmless and can be safely vented into the atmosphere. Its desired function is to complete the electrical circuit in water splitting cells, allowing the capture and storage of electrical energy in the form of H_2 as a chemical fuel and in this way dampening the heavy intermittency of renewable energy fluxes.[16] Its four electron nature means that OER has very sluggish kinetics, especially compared to CER, and the difficulty of catalyzing the reaction poses one of the main barriers preventing widespread implementation of water electrolysis for energy storage.[17−19] In fact, the facile CER kinetics relative to OER is what makes it possible to vigorously evolve chlorine in acidic aqueous media with a pH lower than ∼2, with minimal anodic decomposition of the aqueous solvent.

In a practical sense, it is difficult to envision a situation where the mixed evolution of both chlorine and oxygen is an attractive outcome. Whereas chlorine as a product is unwanted during water electrolysis due to its environmental toxicity, OER is unwanted in chlor-alkali since the oxygen represents a safety risk and its formation is linked to catalyst degradation.[15,20−22] Thus, studying the selectivity between these two highly relevant reactions is important, especially since an OER-selective anode would allow the direct splitting of saline water without the costly need of removing chloride from the system.[23,24] Although OER and CER seem fundamentally different reactions at first glance, it has been often observed that catalyst materials proficient at OER are also highly active for CER, which can be ascribed to a so-called scaling relationship between the binding energies of their key intermediates.[25−27] Such a relationship implies that OER and CER are linked on a fundamental kinetic level, perhaps in the form of a common intermediate surface species and/or a shared active site.[28−30] It also implies that control over selectivity between the two reactions can be a serious challenge. It may be exceedingly difficult, if not impossible, to efficiently separate the two reactions on the basis of kinetic considerations alone, such as by finding an appropriate catalyst.[31−33]

Both CER and OER are most readily catalyzed on metal oxides.[25,34] CER is usually carried out in acidic media because of thermodynamic restrictions (see eq 2), on anodes made of mixtures of RuO_2 and TiO_2, so-called dimensionally stable anodes (DSA).[9] OER can be carried out in a wide pH range, but performance wise, the current state of the art is represented by polymer electrolyte membrane (PEM) electrolyzers which employ acidic pH and are equipped with Ir-based mixed metal oxides.[1] Ir, either as a pure oxide or as a dopant, is the only material known to retain long-term stability during acidic OER operation, and virtually no acidic OER anode is known that does not rely on Ir.[35] Unfortunately, the scarcity of Ir is a crippling limitation to large-scale implementation of PEM electrolyzers, and a large body of research has been devoted to reducing the needed Ir loading, such as by increasing the active surface area or developing Ir-based materials with higher intrinsic activity.

A recent example of Ir-based materials with lower intrinsic Ir mass loading are Ir-based double perovskites, aiming to reduce the amount of Ir needed while retaining the high catalytic OER performance.[36] Previous work by some of us showed that the high OER performance of these materials is related to their instability in acid, leading to amorphization of the surface and formation of a highly active surface layer.[37] An interesting question is how these Ir-based double perovskites perform as

CER electrocatalysts and how parallel CER impacts their stability. They represent an attractive system of study also because of the possibility of studying a series of closely related structures. The Ir double perovskite structure is represented by A_2BIrO_6 and allows a degree of freedom in the type of A and B cations, meaning that many different perovskites can be prepared.

In this work, we explore parallel OER and CER on a series of double perovskites and investigate their selectivity and stability as well as the interdependence between the two reactions in acidic media of pH ∼ 1. Under these conditions, the OER and CER have similar onset potentials and they are in direct kinetic competition. Additionally, the acidic environment allowed the use of an RRDE method to deconvolute parallel OER and CER currents, by using a Pt ring to quantitatively detect Cl_2 evolved on the disk, as described in detail in a previous publication.[38] Relatively low chloride concentrations $(0 < [Cl^-] < 120$ mM$)$ were chosen to study the CER, since it was previously shown that competition between OER and CER is the most prevalent under these conditions.[38] We studied a series of double perovskites written as Ba_2BIrO_6, where B = Pr, Nd, La, Sn, Y, Tb, and Ce. The material Sr_2YIrO_6 was also included with the aim to vary the A cation. Commercial IrO_2 was included as reference material.

2. EXPERIMENTAL SECTION

2.1. Chemicals. $HClO_4$ (60%) and NaCl (EMSURE/ Analysis grade) were purchased from Merck. Ir-based double perovskites were synthesized as reported previously.[36] IrO_2 nanoparticles (Premion, 99.99%) were purchased from Alfa-Aesar. All purchased chemicals were used as received. The water used for all experiments was prepared by a Merck Millipore Milli-Q system (resistivity 18.2 MΩ cm, TOC < 5 ppb).

2.2. Synthesis of the Double Perovskites and X-ray Powder Diffraction. Samples of A_2BIrO_6 (A = Ba and Sr; B = lanthanides, Y, and Sn) were prepared from $BaCO_3$, $SrCO_3$, La_2O_3, CeO_2, Pr_6O_{11}, Nd_2O_3, Tb_4O_7, Y_2O_3, SnO_2, and Ir metal using methods based on standard solid-state reactions.[39,40] The La_2O_3 and Nd_2O_3 powders were preheated at 950 °C overnight before use. The well-ground mixtures were placed in alumina crucibles and allowed to react at 800 °C overnight. The resultant powders were then sintered at 1250 °C for 2 days with intermittent regrinding, and finally, the samples were furnace cooled to room temperature. Every synthesis was carried out in air.

X-ray powder diffraction patterns were collected on a Philips X'Pert diffractometer in Bragg−Brentano geometry, equipped with a X'Celerator detector and a Cu−Kα source. Diffraction patterns were collected in steps of $2\theta = 0.020°$, with a 10 s counting time per step in the range $15° < 2\theta < 90°$.

2.3. Online Electrochemical ICP-MS Analysis. Investigations of the chloride impact on the stability of iridium based double perovskites were performed using an electrochemical scanning flow cell (SFC) with online inductively coupled plasma mass spectrometry (ICP-MS) analysis to detect dissolution products in direct correlation to potential and current density. The SFC is a small polycarbonate cell with an electrolyte flow of 192 μL min^{-1} able to perform classical three electrode electrochemical experiments. The cell's inlet is connected to a counter electrode compartment, housing a graphite rod (Sigma-Aldrich, 99.995%), while a Ag/AgCl reference electrode (Metrohm) is connected by a separate channel directly to the working electrode. The reference electrode was calibrated vs the

RHE, against which all potentials are reported. The working electrode can be moved with an *xyz*-stage (Physik Instrumente, M-403), which allows fast screening of multiple catalyst spots on a glassy carbon plate (HTW, SIGRADUR G, 5 cm × 5 cm). The outlet of the SFC is connected to the ICP-MS (PerkinElmer, NexION 350x) to detect dissolution products. The ICP-MS was calibrated for the elements A, B, and Ir with a four point calibration slope by adding specific amounts of standard solutions (Merck, Certipur, Ir, Pr, Y, Ba, Sr) to the electrolyte. More details about the online SFC ICP-MS system can be found in previous publications.[41−43] The SFC was operated using 0.1 M $HClO_4$ (Merck, Suprapur) as an electrolyte in control experiments, and addition of 50 mM NaCl (Sigma-Aldrich, 99.5%) provided information on chloride impact on the stability. Catalysts were dropcasted from water based suspensions containing 0.27 mg(Ir)/mL and 20 μL of Nafion (Sigma-Aldrich, 5 wt % in aliphatic alcohols). Using 0.3 μL of those suspensions for dropcasting resulted in dried catalyst spots whose sizes (see Table S1) were measured using a Keyence laser profilometer (VK-X200 series). Surface area normalization was based on these spot sizes. Each measurement was carried out in duplicate to ensure reproducibility; data from single measurements are reported.

2.4. General Electrochemical Procedures. All experiments were carried out at room temperature (∼20 °C). Electrochemical experiments were done using homemade two-compartment borosilicate glass cells with solution volumes of 100 mL. Before first-time use, all glassware was thoroughly cleaned by boiling in a 3:1 mixture of concentrated H_2SO_4 and HNO_3. When not in use, all glassware was stored in a 0.5 M H_2SO_4 solution containing 1 g/L $KMnO_4$. Before each experiment, glassware was thoroughly rinsed with water and then submerged in a dilute (∼0.01 M) solution of H_2SO_4 and H_2O_2 to remove all traces of $KMnO_4$ and MnO_2. The glassware was then rinsed three times with water and boiled in water. The rinsing−boiling procedure was repeated two more times.

An IviumStat potentiostat (Ivium Technologies) was used during electrochemistry experiments. All experiments except voltammetric characterizations were 85% *iR*-compensated in situ. The solution resistance was measured with electrochemical impedance spectroscopy at 0.75 V vs RHE by observing the absolute impedance in the high-frequency domain (100−50 kHz) corresponding to a zero-degree phase angle.

2.5. Rotating Ring-Disk Electrode (RRDE) Procedures. RRDE experiments were performed in 0.1 M $HClO_4$ solutions with a pH value of 1.20 ± 0.05, as measured with a Lab 855 m equipped with a glass electrode (SI Analytics). The solutions were saturated with Ar (Linde, purity 6.0) before experiments. Solutions were bubbled with Ar gas during forced convection experiments, and Ar was used to blanket the solution in stationary conditions. The reference electrode was a HydroFlex reversible hydrogen electrode (Gaskatel), separated from the main solution using a Luggin capillary, to fix the reference sensing point and to prevent mixed potentials at the reference due to dissolved Cl_2 gas. The Luggin tip was distanced ∼2 cm from the working electrode to minimize distortion of the current distribution across the electrode surface,[44] and it was aligned to the center of the working electrode, to minimize electrical cross-talk.[45,46] All potentials in this paper are reported on the RHE scale. A Pt mesh was used as a counter electrode, separated from the main solution with a coarse sintered glass frit.

RRDE measurements were done with a MSR rotator and E6 ChangeDisk RRDE tips in a PEEK shroud (Pine Research). GC disks (Pine Research Instrumentation, surface area 0.196 cm^2) were prepared to a mirror finish by hand polishing on Microcloth pads with diamond paste suspensions down to a 0.05 μm particle size (Buehler), followed by rinsing and sonication of the electrode in water for 3 min. The fine-ground catalyst powders were prepared as suspensions of 3 mg/mL (total catalyst mass) in EtOH (AR/Analysis grade, Acros Organics). After drying the prepared GC surface with compressed air, the RRDE tip was placed upside down in the MSR rotator. Thin films of catalyst were prepared by dropcasting 2.5 μL well-stirred EtOH suspension (formal loading ∼38 μg $cm^{−2}$, total catalyst mass) onto the GC surface, followed by drying under rotation at 175 rpm. After the solvent had visibly evaporated, the surface was further dried with hot air for several minutes.

Before any RRDE experiment, the Pt ring was electrochemically reactivated by scanning from −0.1 to 1.7 V at 500 mV $s^{−1}$ for 20 scans at 1500 rpm. Hydrodynamic experiments were done at 1500 rpm by scanning the disk electrode in the range of 1.3−1.55 V at 10 mV $s^{−1}$. In between experiments, the disk electrode was kept at 1.3 V. Ring currents were corrected for constant background currents and product collection delay. The latter arises from the time needed for products formed on the disk to reach the ring, and was approximately 200 ms at 1500 rpm.

The liquid phase collection factor of the ring-disk system, N_l, was determined by studying the $Fe[CN]_6^{3−}/Fe[CN]_6^{4−}$ redox couple in a solution of 10 mM $K_3Fe[CN]_6$ and 0.1 M KNO_3, using the Pt ring with a freshly prepared blank GC electrode. The value was 0.241 within 5% accuracy. The collection factor for dissolved Cl_2 was also measured in the same setup, by evolving chlorine selectively on Ba_2PrIrO_6 in 0.1 M $HClO_4$ + 0.1 M NaCl at a potential of 1.48 V vs RHE, right before the kinetic onset of OER. The collection factor for dissolved chlorine, N_{Cl_2}, was found to be 0.215 within 3% accuracy, slightly lower than N_l. The difference can be attributed to the higher solution pH compared to previous studies,[38] which causes an increase in the degree of Cl_2 dissociation into $Cl^−$ and HClO, the latter of which is not detectable using present methods. The value for N_{Cl_2} was used in all calculations concerning OER and CER current separation.

2.6. Parallel OER and CER: Activity Measurements. Before initiating quantitative measurements, the GC-supported thin films were scanned 20 times in chloride-free 0.1 M $HClO_4$ between 1.3 and 1.55 V, into the OER region, at 1500 rpm. This was done to ensure unchanging catalyst behavior during the experiments. The Pt ring was initially deactivated. The final scan of this procedure was taken as the data for "pure" OER activity. In the next step, the double layer capacitance was determined to allow a degree of normalization of the currents vs electrochemical surface area (see below). Finally, 20 mM NaCl was added to the solution, and the GC supported thin film was scanned once again between 1.3−1.55 V at 1500 rpm, with the Pt ring fixed at 0.95 V vs RHE for Cl_2 detection. These three steps were performed right after one another using the same film and setup. The procedure of steps was repeated for each catalyst material at least three times, in independently prepared solutions and glassware, and using freshly prepared electrode films.

Measurement of the double layer capacitance $(C_{dl})_E$ was done by scanning the electrode in the potential window of 0.05−0.15 V at scan rates of 25, 50, 75, and 100 mV/s (see Figure S7). The value of the double layer capacitance $(C_{dl})_E$ was calculated from the slope of the charging current around 0.1 V vs scan rate,
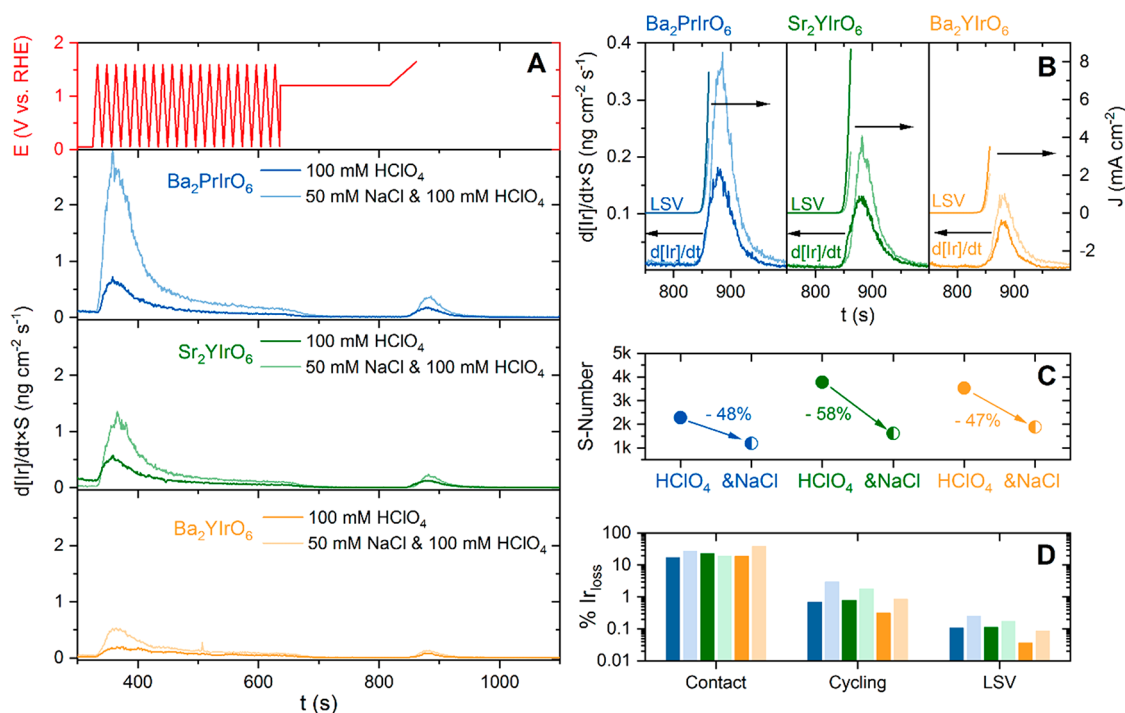
Figure 1. Online electrochemical iridium dissolution from ICP-MS measurements. Panel A, Ir dissolution over time correlated with the applied E vs t protocol (red) for Ba_2PrIrO_6 (blue), Sr_2YIrO_6 (green), and Ba_2YIrO_6 (yellow) in 0.1 M $HClO_4$ (solid) and 0.1 M $HClO_4$ with 50 mM NaCl (pale). For clarity reasons, the initial contact peak is not shown (see Figure S 1 for the full version). Panel B, Ir dissolution along with the current density of the LSV of the E vs t protocol. Panel C, S-number (amount of gases evolved per amount of Ir dissolved) comparison in the presence and absence of 50 mM NaCl. Panel D, total dissolved amount of Ir during initial contact with the electrolyte, cycling, and the LSV, as determined from the initial spot loading (see also Table S 1).

$i_{(C_{dl})_{0.1V}} = (C_{dl})_{0.1V} \times \nu$ (see Figure S8). From $(C_{dl})_{0.1V}$, the electrochemical surface area could be approximated for each individual experiment by normalizing the activity to the specific capacitance of the double layer, assuming 0.059 mF cm^{-2} for the latter.[47] Reported values for each type of catalyst are averaged from individually normalized activities.

2.7. Parallel OER and CER: CER Selectivity vs [Cl$^-$] Measurements. Just like the activity measurements, the GC-supported thin films were scanned at least 20 times in chloride-free 0.1 M $HClO_4$ between 1.3 and 1.55 V at 1500 rpm to ensure unchanging catalyst behavior during experiments. Following this, the ring was activated and kept at 0.95 V vs RHE during all measurements. The electrode was then again scanned between 1.3 and 1.55 V at 1500 rpm, while increasing the concentration of NaCl in steps from 0 mM to 120 mM. No attempt at normalization versus surface area was undertaken for these experiments, since we were interested in OER vs CER selectivity and their reaction orders only, which are not affected by current normalization. Details about the preparation of an amorphous, hydrated IrO$_x$/GC catalyst can be found elsewhere.[38]

3. RESULTS AND DISCUSSION

3.1. ICP-MS Measurements and Effect of Chloride on Stability. A series of Ba_2BIrO_6 compounds (B = Pr, Nd, La, Sn, Y, Tb, Ce) and Sr_2YIrO_6 were synthesized and investigated for OER and CER activity and selectivity. We first investigated the stability of these materials under representative electrochemical conditions, since it has recently been shown that Ir-based perovskites are unstable in acidic media. Ba_2PrIrO_6[36,37] and the single perovskite $SrIrO_3$[48] tend to leach out both Ir and non-noble metals from their lattice during sustained OER, leading to

an amorphous IrO$_x$ outer surface layer that is highly active toward OER, expectedly more so than the bulk material. The main driver for this instability appears to be the favorable thermodynamics of non-noble metal dissolution in acidic media, followed by codissolution and/or collapse of the interspaced IrO$_6$ octahedra. Since our experiments involve CER in addition to OER, it was necessary to study the effect of chloride on the leaching behavior of the studied materials.

We performed online electrochemical ICP-MS measurements to follow the dissolution of Ir and the A + B cations under electrochemical conditions in 0.1 M $HClO_4$, in presence and absence of 50 mM NaCl. Each experiment was comprised of the same electrochemical protocol seen in Figure 1A (top). Contact was made at 0.05 V, while subsequent potential cycling at 200 mV s^{-1} to 1.6 V was used to reach reproducible CVs. After a "resting" period at 1.2 V in which the dissolution subsided to its background signal, a linear sweep voltammogram (LSV) at 10 mV s^{-1} to 1.65 V, along with the integral of Ir dissolution, was used to calculate the stability number (S-number).[37] In the presence of chlorides, the formula for calculating the S-number was adapted according to eq (S 1) to include the formation of chlorine gas. Ba_2PrIrO_6, Ba_2YIrO_6, Sr_2YIrO_6, and Ba_2CeIrO_6 were chosen as representative double perovskites.

Figure 1 summarizes online ICP-MS Ir dissolution from Ba_2PrIrO_6, Ba_2YIrO_6, and Sr_2YIrO_6 during the electrochemical protocol; additional dissolution data for Ba_2CeIrO_6 is shown in the Supporting Information. Similar to a previous report,[37] all materials experience major Ir leaching immediately upon contact with the acidic electrolyte (Figure 1D), during which the electrode is conditioned at 0.05 V vs RHE. Cycling of the electrode promotes the rate of iridium leaching, suggesting that the effect is strongly dependent on transient changes in the
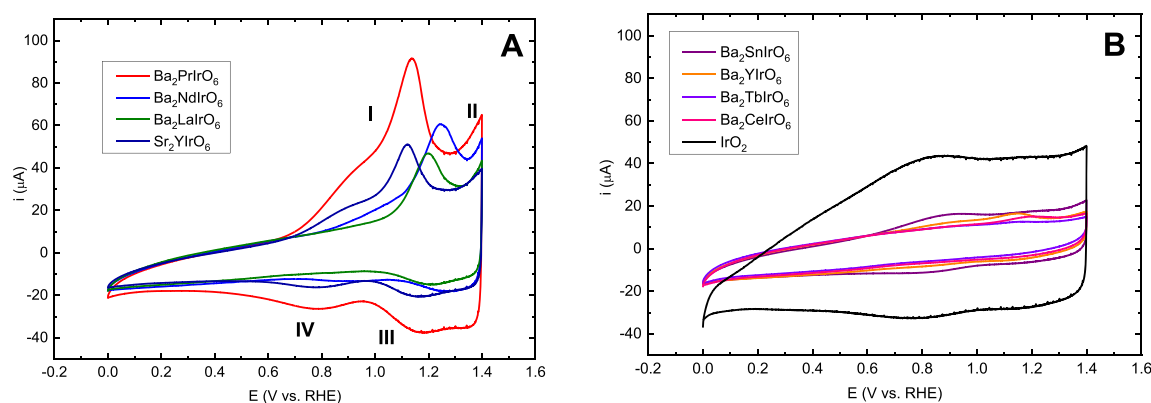
Figure 2. Voltammetric characterization of the Ir-based double perovskites used in this study, in a 0.1 M $HClO_4$ solution, supported on GC. All materials were scanned at least 20 times in the range of 1.30−1.55 V at 1500 rpm prior to characterization. Catalysts are shown in groups with pronounced Ir redox transitions (A) and those with less obvious features, plus the IrO_2 reference (B). Scan rate: 50 mV s^{-1}.

catalyst matrix.[49] Non-noble components (Ba, Pr, Sr, Y, and Ce) on the other hand show little to no potential dependent dissolution and merely dissolve upon electrolyte contact. Table S 2 offers an overview of all integrated dissolution rates. In this table, Ba_2PrIrO_6 in chloride-free electrolyte shows enhanced contact dissolution rates of Ba compared to Pr and Ir; this conforms to previously reported XPS data on Ba_2PrIrO_6 which was exposed to a similar environment.[36] Interestingly, Sr in Sr_2YIrO_6 shows a small but more pronounced potential dependent dissolution during cycling than Ba in Ba_2PrIrO_6 and Ba_2YIrO_6. A lack of a clear trend for the total dissolution of any element in the presence of chloride is due to the big percentage of the contact dissolution on the overall dissolved amount (90−100%). Since the contact peak is rarely reproducible for the same catalyst as it depends on many factors, we only discuss dissolution during potentiodynamic control in the following. Most importantly, the dissolution of Ir is increased significantly during both the cycling and the linear potential ramp (Figure 1D). To look into this aspect in more detail, the extent of Ir leaching was correlated with the catalytic current in the voltammogram during the final LSV (Figure 1B). This allowed the calculation of the S-numbers for both pure OER in $HClO_4$ as well as a competitive OER and CER in the presence of chloride (Figure 1C). A faradaic efficiency of 100% toward OER and 90% CER to 10% OER was assumed according to RRDE experiments, respectively (see below). The stability number S (plotted in Figure 1C) had a very similar value for Ba_2PrIrO_6, Ba_2YIrO_6, and Sr_2YIrO_6. For Ba_2CeIrO_6, OER activity and Ir dissolution during the linear sweep were too low to accurately measure, and S could not be determined. In the presence of chloride, all materials experience more Ir dissolution, as illustrated by a roughly 50% decrease in S, which is in line with previous results on the stability of noble metals such as Pt and Rh in the presence of chloride.[50] These results suggest that the dissolution of noble metal centers is impacted very differently during CER than during OER. We speculate that whereas during OER, the dissolution is driven by formation of higher oxide species, Cl$^-$ may enhance Ir dissolution specifically by forming chloro-iridate complexes such as $IrCl_3$ and $Ir[Cl]_6^{3-}$. We note that the total amount of Ir that dissolved from the double perovskites during these experiments is several orders of magnitude larger than what has been reported for IrO_2.[51] This means that IrO_2 represents an interesting, transiently stable material for comparison in this study.

3.2. Catalyst Characterization. To verify the bulk properties of the materials tested in this study, powder XRD patterns were measured (Figure S 2). The patterns generally agree with those reported in the literature;[39,40,52] in particular, the presence of the super lattice lines at about 18° and 35°, which in the double cubic cell are indexed as (111) and (311), respectively, suggest an ordered arrangement of the BO_6 and IrO_6 octahedra. The IrO_2 shows poor crystallinity, displaying a single broad peak of overlapping rutile (110) and (101) reflections around 28° and 35° as well as a wide (200) reflection around 40°. A trace of metallic Ir is also present; this trace disappeared quickly upon cycling (see Figure S 4).

For the RRDE measurements, ethanol suspensions of the fine powders were dropcasted directly onto polished GC substrates and dried, followed by submersion and electrochemical measurements. We avoided the use of binders such as Nafion,[36,53,54] since it was found that Nafion had a major depressing effect on CER selectivity, likely due to its permselective behavior for cations (see Figure S 3).[55] ICP-MS control experiments showed that Nafion slightly enhanced Ir dissolution in Ba_2PrIrO_6 during the electrocatalytic LSV (Table S 2); the S-number however decreased very similarly (−47% vs −48%) under the effect of chloride. These results suggest that dissolution is much less strongly affected by chloride mass transport than the CER. Figure 2 displays the voltammetric characterization of ~38 μg cm^{-2} formal catalyst mass loadings of the investigated double perovskites and IrO_2 in the potential window of 0−1.4 V.

On the basis of the stability results (section 3.1), we expect transient dissolution in all double perovskites during the RRDE measurements. All characterizations in Figure 2 were therefore taken from electrodes that were scanned at least 20 times in the potential region 1.30−1.55 V in 0.1 M $HClO_4$ at a rotation rate of 1500 rpm to ensure that the voltammograms correspond to the actual catalyst surfaces that were used for subsequent OER and CER catalysis. The plots cannot be ascribed to idealized double perovskite surface structures but should be considered as double perovskite-derived thin IrO_x films in varying states of amorphization.

On the basis of their voltammetric characterization, we divided the materials into two groups. First, we consider Ba_2PrIrO_6, Ba_2NdIrO_6, Ba_2LaIrO_6, and Sr_2YIrO_6, which show strong redox transitions in the range of 0.6−1.4 V (Figure 2A). These transitions are tentatively ascribed to Ir redox transitions, as was done previously for Ba_2PrIrO_6.[37] Ba_2PrIrO_6 and Sr_2YIrO_6

show two sets of peaks in the forward scan (marked I and II) and in the backward scan (marked III and IV). Considering the position and irreversibility of the peaks, we ascribe these peaks to the formation of an amorphous IrO_x surface layer as a result of the leaching of A and B cations. Peaks I and IV likely correspond to a transition between Ir^{3+} and Ir^{4+}, whereas peaks II and III represent further Ir oxidation that may be beneficial for OER catalysis (either formation of Ir^{5+} centers[56−58] or the more recently proposed formation of Ir^{4+}-O^- moieties).[59,60] Second, the group of Ba_2SnIrO_6, Ba_2YIrO_6, Ba_2TbIrO_6, and Ba_2CeIrO_6 shows more subtle features (Figure 2B). It is somewhat surprising that Ba_2YIrO_6 and Ba_2CeIrO_6 do not have pronounced Ir redox peaks, since they also displayed significant dissolution upon contact in ICP-MS measurements (Table S 2). Possibly, an amorphous IrO_x layer is formed not during contact dissolution but during potential scanning in the OER region; the rate of Ir dissolution during this scanning, which differs between catalysts, perhaps controls the extent to which the layer forms. The IrO_2 reference shows a broad profile with small reversible peaks around 0.8 and 1.2 V, in accordance with previous studies on IrO_2.[61] We observed a trace of hydrogen evolution near 0 V for "pristine" IrO_2 before scanning repeatedly into OER, which we ascribe to a small amount of metallic Ir present in the bulk (see also Figure S 4). This behavior is no longer visible in Figure 2B because of the irreversible conversion of interfacial metallic Ir into its oxide, which is a much worse HER electrocatalyst.[62] See Figure S 4 for comparisons of the curves in Figure 2 with the catalysts in their "pristine" state.

We must note that, in the context of this paper, the focus is on selectivity and OER/CER interdependence, meaning we are not interested in absolute activities per se. It is however still desirable to apply normalization of current vs the catalytically active surface area to allow comparison between different catalysts, even though the "active site" could become ambiguous in the case of two distinct reactions. The most common and straightforward approach is normalization vs the electrochemically active surface area (ECSA) by measuring the double layer capacitance $(C_{dl})_E$ around potential E, which is expected to scale with the ECSA according to

$$ECSA = \frac{(C_{dl})_E}{C_{dl}^*} \tag{3}$$

where C_{dl}^* is the specific capacitance per surface area of the material. $(C_{dl})_E$ can be determined from the slope of the double layer charging current vs the scan rate (Figure S 7). Unfortunately, accurate ECSA determination is a persistent problem throughout electrocatalysis,[63] for four main reasons: (i) accurate values of C_{dl}^* generally do not exist, (ii) $(C_{dl})_E$ has to be measured in a region completely free of faradaic processes, (iii) $(C_{dl})_E$ may be affected by the (potential-dependent) conductivity of the material, (iv) determination of $(C_{dl})_E$ is not a selective chemical surface titration method, so that its value may actually not be the best measure of the ECSA.

Ideally, $(C_{dl})_E$ should be measured at the same potential for all materials. Considering Figure 2, there is large variation in behaviors for the studied materials within the potential window of 0−1.4 V; the Ir-related redox transitions in Figure 2A are visible in a wide potential range up until the OER/CER onset, meaning that any $(C_{dl})_E$ measurement in this potential range is distorted by pseudocapacitive contributions. McCrory et al. recommend measuring C_{dl} around the open circuit potential, but almost all measured materials assumed an open-circuit potential

value that fell in the pseudocapacitance area. In fact, the E_{OCP} value is likely not suitable in this regard, since it almost invariably depends on mixed potentials, i.e., the occurrence of multiple surface reactions resulting in zero net-current. Other authors recommend electrochemical impedance modeling to measure the adsorption capacitance of reaction intermediates as an estimate of the ESCA.[64] In the end, we resorted to measuring $(C_{dl})_E$ in a 0.1 V interval centered around 0.1 V, hereby termed $(C_{dl})_{0.1V}$; this area appeared free of pseudocapacitive processes for all materials (Figure 2). Assuming a specific capacitance $C_{dl}^* = 0.059$ mF cm^{-2}, an "average" of reported literature values for oxides in acidic conditions,[36,47] we obtained ECSAs with similar magnitudes as the geometrical surface area. The caveat of this method is the large separation of OER-relevant potentials and the ECSA determination. Under the assumption that the Ir centers dictate the observed pseudocapacitive behavior, we also cannot exclude interference from conductivity (category (iii)), since amorphous Ir oxides show a notable decrease of conductivity below 0.5 V.[65] In effect, this means that part of $(C_{dl})_{0.1V}$ may originate from the GC substrate.[66,67] Despite the shortcomings of this normalization method, we again note that the activity normalization affects neither the slope of Tafel curves, the reaction order analysis, or OER vs CER selectivity.

3.3. OER and CER Activity Trends. In consideration of sections 3.1 and 3.2, we will not theorize about catalyst structure vs catalytic activity relationships, since the true structure of the double perovskite surfaces is not known. The materials show rather diverse catalytic behavior as will be shown below.

During scanning rotating ring-disk electrode (RRDE) voltammetry involving parallel CER and OER, the two reactions can be separated by using eq 4:

$$i_{OER} = i_D - i_{CER} = i_D - \frac{|i_R|}{N_{Cl_2}} \tag{4}$$

In eq 4, the total current on the disk electrode i_D is assumed to be the sum of CER current (i_{CER}), OER current (i_{OER}), and a residual current originating from scanning (pseudo)capacitance. The capacitive contribution can be effectively minimized by using a relatively slow scan rate of 10 mV s^{-1} and averaging forward and backward scans, yielding approximately only catalytic current from catalytic OER and CER (i_D), which are solution-controlled processes. We were then able to separate the CER current contribution by fixing the potential of the Pt ring at 0.95 V vs RHE to selectively detect Cl_2 evolved on the disk (where reducing current is thus measured). The obtained ring current (i_R) is directly proportional to CER rates. A further correction for the ring collection factor of chlorine ($N_{Cl_2} \approx 0.215$ in 0.1 M $HClO_4$) yields i_{CER}, the CER current contribution. The remaining current on the disk was then assumed to originate from OER. See Figure S 5 for an example curve measured during a typical experiment.

Due to the perceived instability of the catalysts under study, we must note that the ring measurements may be affected by dissolved species coming from the disk. These species could cause additional stray reduction reactions or interfere with Cl_2 detection by redepositing as species which are not active toward Cl_2 reduction. As evidenced by their Pourbaix diagrams,[68] most A and B cations used in this study are expected to be electrochemically inert at 0.95 V in acidic solution, meaning they will not react or deposit on the Pt ring. Only Sn and solution-phase iridium species may possibly deposit as oxides under the studied conditions. From the Ir dissolution rates in
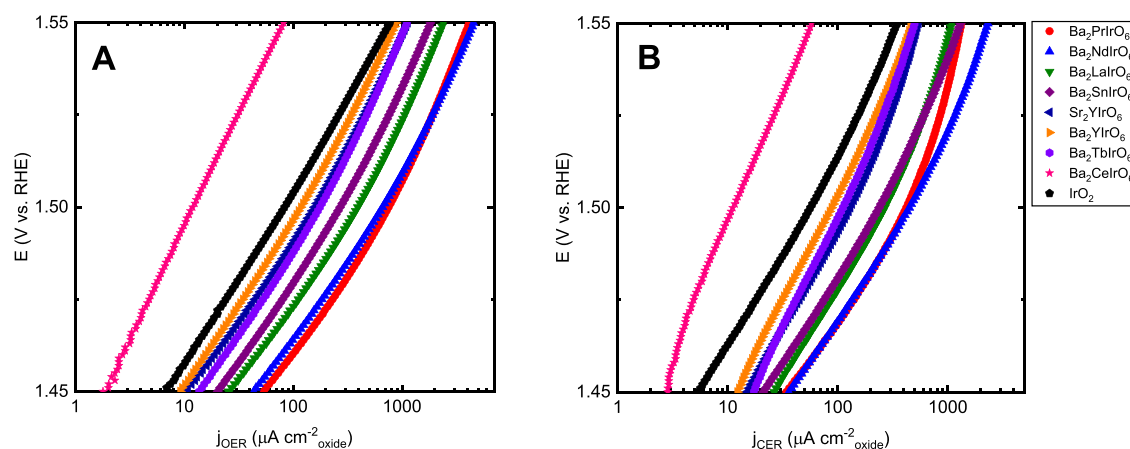
Figure 3. OER (A) and CER (B) Tafel curves obtained by scanning the electrode between 1.30 and 1.55 V at 10 mV s^{-1}: (A) "pure" OER current densities in a 0.1 M HClO$_4$ solution and (B) CER current densities in a 0.1 M HClO$_4$ + 20 mM NaCl solution, derived from ring currents on a Pt ring fixed at 0.95 V vs RHE. Values shown are the average of at least three independent measurements (see Figure S 9 for a version containing error bars). Solutions saturated with Ar, rotation rate 1500 rpm.
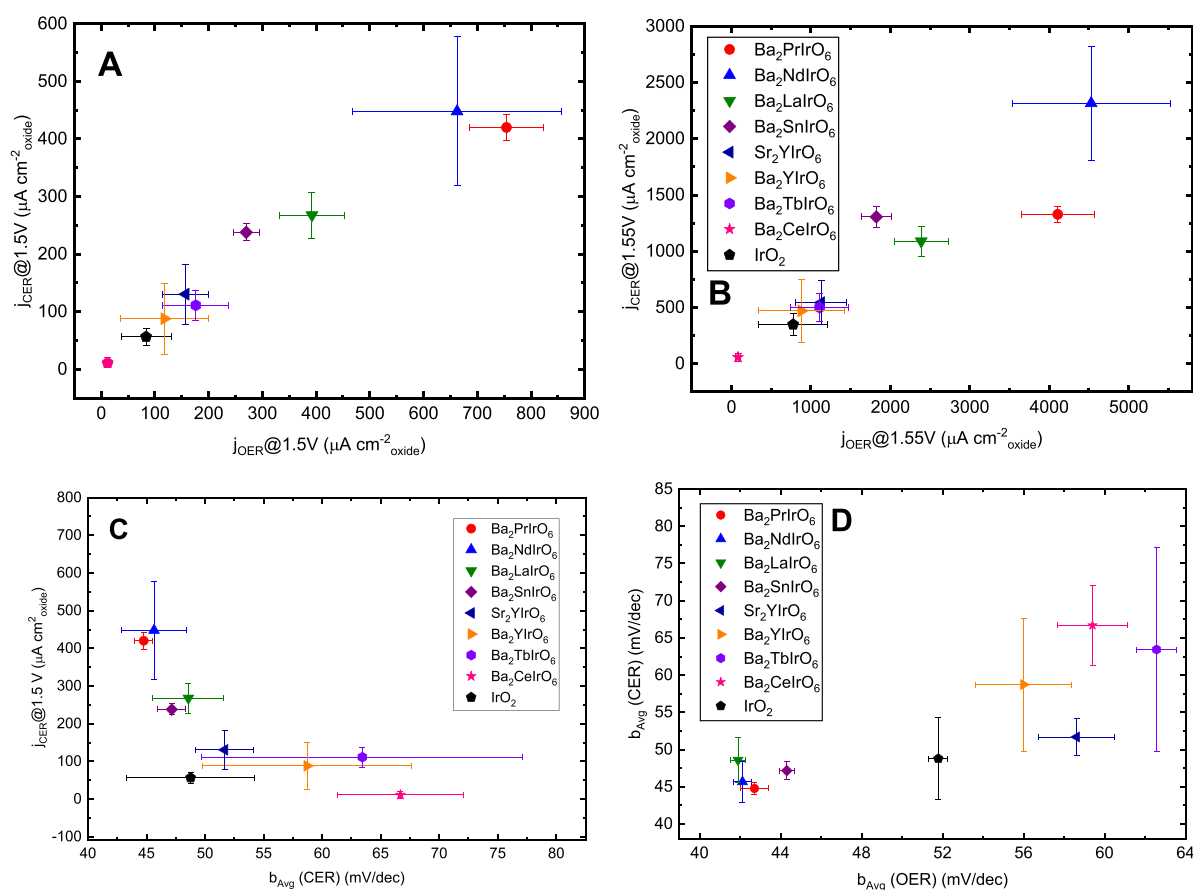

Figure 4. Correlations between OER and CER activities, data derived from Figure 3 (CER measured in 20 mM NaCl). (A and B) OER vs CER current densities compared at 1.50 and 1.55 V, respectively. (C) Comparison of CER Tafel slope vs current densities measured at 1.50 V, the upper potential limit of the linear portion (see also Figure 3B). (D) Comparison of Tafel slopes from linear portions (1.45−1.50 V) of OER and CER. All data are averages of at least three independent measurements; error bars represent corresponding standard deviations.

ICP-MS measurements, we estimate that the error due to reduction reactions involving Ir is at least 2 orders of magnitude lower than the smallest ring currents related to CER (Figure S 6). Furthermore, a rough estimate shows that it would take at least 10 min of continuous operation at high potential to form a perfect IrO$_2$ monolayer on the ring. Serious interference at the

Pt ring can thus be safely excluded (see the Supporting Information for full details).

The value of the Tafel slope has been used as a "benchmark" for catalytic OER performance, with a lower Tafel slope correlating with a "better catalyst".[69−71] It must be noted that strictly speaking, the catalytic performance of a material is not governed by the Tafel slope only. A low Tafel slope is only
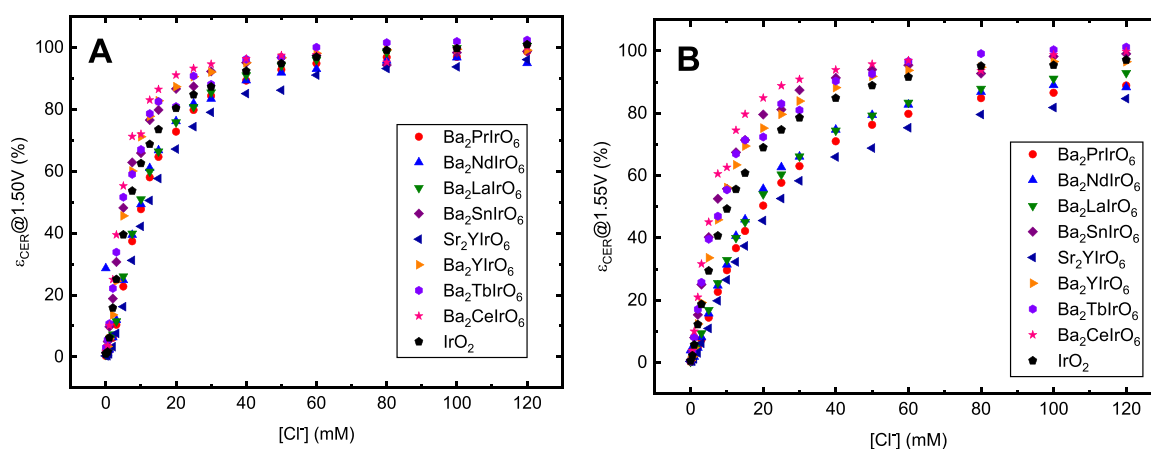
Figure 5. CER selectivity (ε_{CER}, definition in main text) as a function of $[Cl^-]$ for different Ir double perovskites and the IrO_2 reference. Values shown at 1.50 V (A) and 1.55 V (B). Values were obtained with the RRDE method as described in Figure 2.

favorable if it leads to a low(er) overpotential at the desired current density. We will discuss our experimental findings related to the Tafel slope in this spirit, namely, that catalytic performance and the Tafel slope are not by definition correlated.

We first set out to measure "pure OER" currents (in the absence of Cl^-) as well as CER currents measured during parallel OER and CER. Figure 3A shows OER Tafel plots constructed from capacitance-corrected disk current densities, in the absence of Cl^-. Figure 3B shows CER Tafel plots constructed from ring currents in the presence of 20 mM Cl^-. The activities for OER roughly follow the order Pr ≈ Nd > La > Sn > Sr_2Y ≈ Tb > Ba_2Y > IrO_2 > Ce. The most catalytically active DPs Ba_2PrIrO_6, Ba_2NdIrO_6, Ba_2LaIrO_6, and Sr_2YIrO_6 also show a redox transition in their blank CVs (see Figure 2A); we speculate that activities correlate to the extent of surface leaching, although a definite correlation between activity and total dissolved amounts could not be established (see sections 3.1 and 3.2). Interestingly, the same order in activity is observed for CER, indicating scaling between OER and CER activities.

To minimize mass transport control in case of CER, the experiments were performed at 1500 rpm. The highest measured CER current densities per geometric area, as measured at 1.55 V on $BaPr_2IrO_6$, were approximately 10% of the theoretical diffusion limited current as predicted by the Levich equation. We thus assume that mass transport effects on CER are negligible in the potential ranges studied. OER is considered effectively immune to mass transport effects.

Figure 4A,B shows a comparison of CER and OER current densities for all materials, plotted at 1.50 and 1.55 V. As already faintly visible from Figure 3, there is a linear scaling relationship between OER and CER activity. Although such a relationship has been observed previously in the literature, it must be noted that this is one of the few reports directly showing a correlation between CER and OER activity among a group of catalysts.[25] Furthermore, all materials, including the least active ones, showed regions of linear Tafel phenomena for both OER and CER ($R^2 > 0.98$). The slopes of these linear CER Tafel sections are shown in Figure 4C, in comparison to CER current densities at 1.50 V. In Figure 4C, a lower Tafel slope correlates with higher CER current densities, which is a reasonable finding due to the exponential nature of the j/E curves. Furthermore, the catalytically most active materials display linear Tafel slopes in the range 45−50 mV/dec for CER and slopes of 40−45 mV/dec for OER (Figure 4D); for the less active materials, higher Tafel

slopes with a higher variance are observed (see Table S 3 for all numerical Tafel slope values).

In light of the instability of the materials, we must comment on the possible origin of the linear relation between OER and CER activity. As previously mentioned, the selective leaching of non-noble A and B cations from the lattice will to a varying extent form an amorphous IrO_x surface layer on all materials. Since the double perovskites share identical structural motifs, one can expect them to follow comparable amorphization behavior. This could result in thin catalytically active IrO_x layers with perhaps varying surface area but similar kinetics, and thus a linear OER vs CER relation would always be observed. However, the variance in Tafel slopes for CER strongly speaks against this effect being the only descriptor for OER and CER activity;[34,72] if identical IrO_x is formed, then all semilogarithmic $i-E$ curves should display nearly identical (±5 mV/dec) Tafel slopes, which is not the case. The IrO_2 reference furthermore fits in the scaling trend very well, despite possessing a rather different structure compared to the double perovskites. All in all, although we cannot discern the true nature and structure of the active catalyst phases, we can still conclude that they vary among catalysts and that despite this, a linear scaling relationship between CER and OER is observed. The origin of the scaling has been commented on by Trasatti.[25] It is possibly a similarity between the way that chloride binds to surfaces, as compared to the several key oxygen intermediates believed to be involved in the OER.[26] Most importantly, scaling suggests that a catalyst with a kinetic preference toward only one of the reactions may be very hard to find.

3.4. CER Selectivity as a Function of Chloride Concentration.
We further probed OER vs CER selectivity of the materials by varying the chloride concentration stepwise between 0 and 120 mM. Molar selectivities toward CER (ε_{CER}) were defined as a ratio of CER current and combined OER and CER current, where the individual CER and OER currents were normalized to the amount of electrons in each reaction (eq 5):

$$\varepsilon_{CER} = \frac{^{1}/_{2}i_{CER}}{^{1}/_{2}i_{CER} + ^{1}/_{4}i_{OER}} \tag{5}$$

Measured values of ε_{CER} for all materials are shown in Figure 5, at 1.50 and 1.55 V.

At 1.50 V (Figure 5A), ε_{CER} is very similar among materials and shows a strong dependence on chloride concentration. At 1.55 V (Figure 5B), selectivity toward OER increases and there
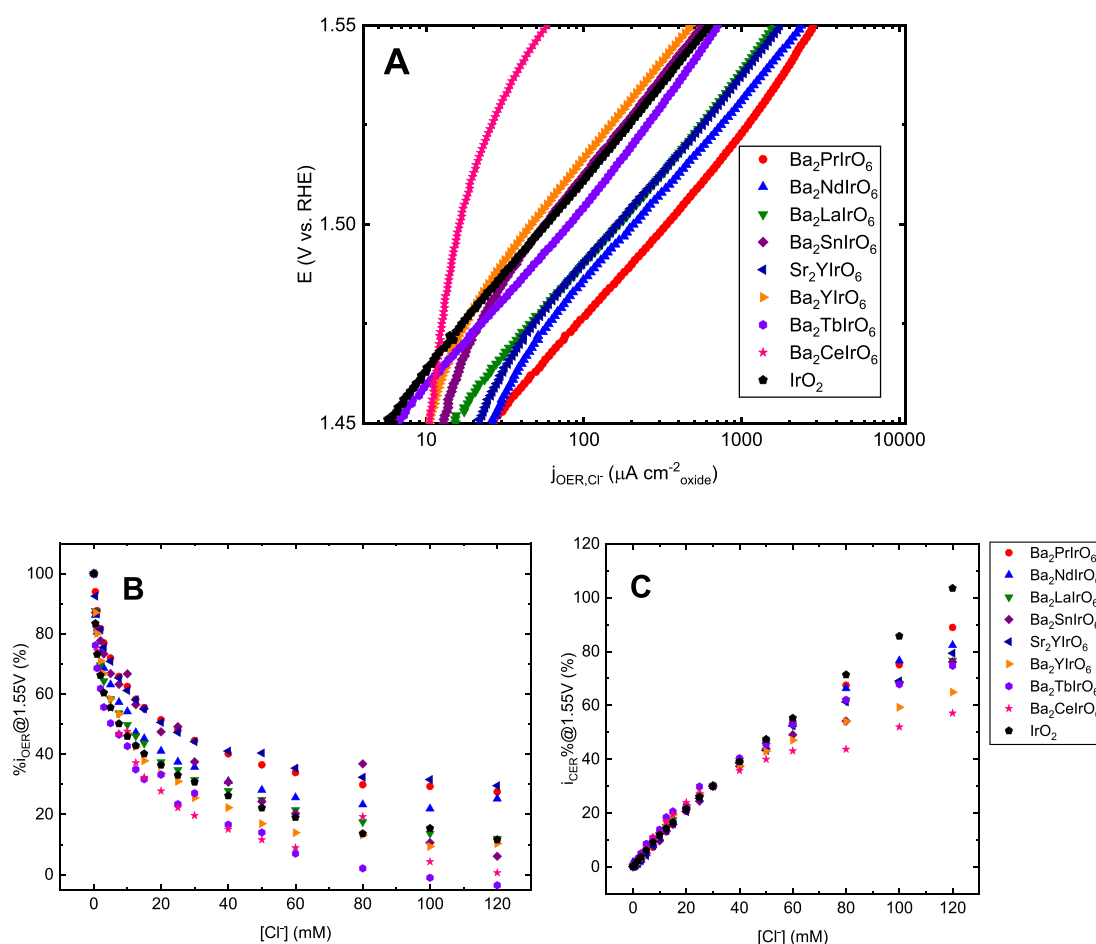
Figure 6. Effect of chloride concentration on OER and CER. (A) OER currents measured in the presence of 20 mM NaCl, in parallel with CER. (B and C) Relative OER current (B) and CER current (C) as a function of increasing chloride concentration. The % OER currents are shown relative to chloride free conditions (0 mM NaCl), and the % CER currents are shown relative to 30 mM NaCl. See Figure S 12 for versions of parts A and B containing absolute currents.

is more variance among materials. A group consisting of Ba_2PrIrO_6, Ba_2NdIrO_6, Ba_2LaIrO_6, and Sr_2YIrO_6 shows particularly high OER selectivity. At both potentials shown, the least active materials generally show higher selectivity toward CER. An important exception is Ba_2SnIrO_6; this material shows relatively high CER selectivity at both 1.50 and 1.55 V while also possessing relatively high activity. Despite these differences, it can be said that ε_{CER} is globally governed by a single relationship; none of the materials show extremely diverging values (>20%) in their selectivity between OER and CER. This conclusion is in-line with Figure 4A,B, where a scaling trend was seen at the single concentration $[Cl^-]$ = 20 mM; this tendency seems to be applicable to higher chloride concentrations as well. The effect of mass transport on the measured CER currents should not be high. A 10% decrease in CER current, the prediction for maximum mass transport control in the experiments (see also the discussion of Figure 3), should lead to a decrease in ε_{CER} of less than 2% for virtually all chloride concentrations. At potentials above 1.55 V, selectivity toward OER will presumably increase, since CER will become increasingly mass transport limited whereas OER is much less affected. We were unfortunately not able to probe this potential region due to formation of persistent O_2 bubbles at high current densities on the electrode tip, which interfered with the collection efficiency.[38]

3.5. OER vs CER Interdependence and Effect of Chloride Concentration.
In this section, we look more deeply into parallel OER and CER as a function of chloride concentration. Figure 6 shows the effect of chloride regarding the OER Tafel curves as well as relative OER and CER activity.

The chloride concentration exhibits a pronounced influence on all catalysts under study regarding both CER and OER. When comparing Figure 6A to Figure 3A, the presence of 20 mM Cl^- induces a shift of the OER Tafel curves toward higher potentials, a reduction in the apparent OER exchange current density, and thus a decrease in OER activity (a factor of 2 for most materials). A scaling relationship was again apparent when OER data from Figure 6A was compared to CER data from Figure 3B (see Figure S 10). Figure 6B,C shows relative OER and CER currents as a function of increasing $[Cl^-]$. For OER, all values are shown as percentages relative to the value at chloride free conditions ($[Cl^-]$ = 0 mM). Likewise, all values for CER are shown relative to $[Cl^-]$ = 30 mM, where the value of the current at this concentration was taken as "30%". This normalization was done due to the different current densities and allows a clearer comparison between trends among materials as chloride concentrations increase (see Figure S 12 for the absolute currents). Figure 6B shows a nonlinear decrease in OER current as a function of $[Cl^-]$ on all materials, in some cases (Ba_2TbIrO_6 and Ba_2CeIrO_6) approaching virtually complete OER suppression at 120 mM. At the same time, all materials show a
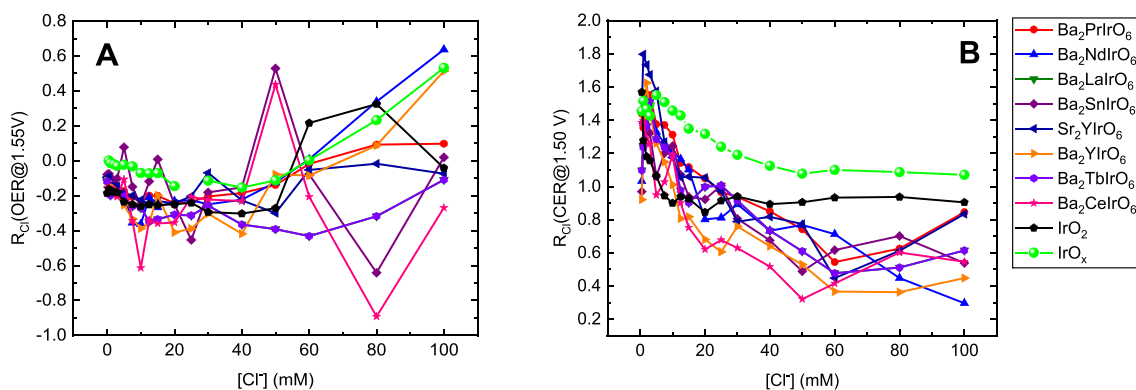
Figure 7. Reaction orders vs chloride concentration ($\mathcal{R}_{Cl^-}$) for OER (A) and CER (B). Values were derived using the $[Cl^-]$-dependent slopes of Figures S 15 and S 16.

continuous CER increase with increasing $[Cl^-]$ (Figure 6C), but there is significant downward curvature in all plots except for the IrO_2 reference.

For further analysis of the interdependence between OER and CER, we consider theoretical models of these reactions and their predictions for chloride reaction orders. As has been comprehensively described by Conway and co-workers,[73] and more recently by Rosestolato et al.,[74] reaction orders (and also Tafel slopes) of reactions involving a chemisorbed intermediate are never expected to remain constant as a function of concentration in the bulk, because of varying surface coverage of the intermediate. In this regard, chlorine evolution is a multistep reaction which involves elementary reaction steps termed Volmer, Tafel, and Heyrovský, which correspond to electrochemical adsorption, recombinatio,n and electrochemical desorption, respectively,

$$Cl^- + * \rightleftarrows Cl^* + e^- \qquad (6)$$

Electrochemical adsorption (Volmer step)

$$2Cl^* \rightleftarrows Cl_2 + 2* \qquad (7)$$

Recombination (Tafel step)

$$Cl^* + Cl^- \rightleftarrows Cl_2 + e^- + * \qquad (8)$$
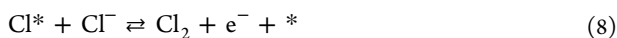
One can additionally consider a mechanism involving a "fourth" elementary reaction, as formulated by Kristhalik:[75]

$$Cl^* \rightleftarrows Cl^{*+} + e^- \qquad (9)$$

$$Cl^{*+} + Cl^- \rightleftarrows Cl_2 + * \qquad (10)$$

This mechanism, in which eq 9 is rate-limiting, involves the formation of a short-lived "chloronium" (Cl^{*+}) intermediate, which is proposed to be stabilized by metal–oxygen groups.[13,76]

In the simplest method of deriving theoretical current–potential relationships from these reactions, the Volmer step is taken as a quasi-equilibrium, with the subsequent rate-limiting step as either recombination or electrochemical desorption. The observed current density then becomes dependent on θ_{Cl}, the fractional surface coverage of chemisorbed intermediate Cl^*.[73] As a further approximation, one can assume that the adsorption of chloride obeys the Langmuir isotherm and that the surface reaction rate follows the mean-field approximation.[77] In the case of a Volmer–Tafel mechanism, the current–potential relation can then be modeled according to

$$j_{VT} = 2Fk_T(\theta_{Cl})^2 = 2Fk_T\left(\frac{K_V[Cl^-]\,e^{f\eta_V}}{K_V[Cl^-]\,e^{f\eta_V} + 1}\right)^2 \qquad (11)$$

In this equation, k_T is the (nonelectrochemical) rate constant for recombination, K_V and η_V describe the chemical quasi-equilibrium constant and overpotential for the Volmer adsorption step, and $f = F/(RT)$. Only the irreversible (activated) potential region is considered, such that the backward reaction may be neglected. From this equation, one can derive $\mathcal{R}_{Cl^-}^{CER}$, the CER reaction order versus $[Cl^-]$ at a constant potential E, as

$$\mathcal{R}_{Cl^-}^{CER} = \left(\frac{\partial \ln i_{VT}}{\partial \ln[Cl^-]}\right)_E = 2(1 - \theta_{Cl}) = \frac{2}{K_V[Cl^-]\,e^{f\eta_V} + 1} \qquad (12)$$

An analogous treatment for consecutive Volmer–Heyrovský steps leads to

$$j_{VH} = Fk_0^H[Cl^-]\,e^{\alpha_H f\eta_H}\theta_{Cl} = Fk_0^H\frac{K_V'[Cl^-]^2\,e^{(1+\alpha_H)f\eta_H}}{1 + K_V'[Cl^-]\,e^{f\eta_H}} \qquad (13)$$

$$\mathcal{R}_{Cl^-}^{CER} = \left(\frac{\partial \ln i_{VH}}{\partial \ln[Cl^-]}\right)_E = 2 - \theta_{Cl} = \frac{K_V'[Cl^-]\,e^{f\eta_H} + 2}{K_V'[Cl^-]\,e^{f\eta_H} + 1} \qquad (14)$$

In these equations, K_V' is again the chemical quasi-equilibrium constant for the Volmer adsorption step (on the potential scale of the Heyrovský step), and k_0^H, α_H, and η_H are the standard rate constant, transfer coefficient, and overpotential for the Heyrovský step. This model predicts that as $[Cl^-]$ increases, θ_{Cl} approaches 1; in the case of a V–T mechanism, $\mathcal{R}_{Cl^-}^{CER}$ varies between 2 and 0. In the case of a V–H mechanism, $\mathcal{R}_{Cl^-}^{CER}$ varies between 2 and 1. The V–K mechanism is reminiscent of the V–H mechanism but predicts that $\mathcal{R}_{Cl^-}^{CER}$ varies between 1 and 0:

$$\mathcal{R}_{Cl^-}^{CER} = \left(\frac{\partial \ln i_{VK}}{\partial \ln[Cl^-]}\right)_E = 1 - \theta_{Cl} = \frac{1}{K_V'[Cl^-]\,e^{f\eta_K} + 1} \qquad (15)$$

The simplest model accounting for the chloride dependence of the OER current would be to assume a simple site blocking, similar to previous work by Fernández et al.:[78]

$$i_{OER} = i_{OER}^0(1 - \theta_{Cl}) = i_{OER}^0\left(1 - \frac{K_V[Cl^-]\,e^{f\eta_V}}{1 + K_V[Cl^-]\,e^{f\eta_V}}\right) \tag{16}$$

In this equation, i_{OER} describes the measured OER current; i_{OER}^0 describes the OER current that would have been measured in absence of chloride. The other symbols again relate to a Volmer-type adsorption of chloride. For the corresponding OER reaction order versus $[Cl^-]$, the dependence is

$$\mathcal{R}_{Cl^-}^{OER} = \left(\frac{\partial \ln i_{OER}}{\partial \ln[Cl^-]}\right)_E = -\frac{K_V[Cl^-]\,e^{f\eta_V}}{1 + K_V[Cl^-]\,e^{f\eta_V}} \tag{17}$$

From this expression, we expect $\mathcal{R}_{Cl^-}^{OER}$ to change from 0 to -1 as $[Cl^-]$ increases, with the rate of change depending on the overpotential and K_V.

The above models all make use of a Langmuir model isotherm for chloride adsorption. In reality, repulsive interactions between adsorbed chloride (and halides in general) will exist.[77] If this is taken into account by using a Frumkin isotherm, this will lead to a broadening of the isotherm, i.e., a broader range of chloride concentrations is needed to reach maximum coverage. For the models described above, this implies that the basic predictions remain the same and only that the predicted change from one reaction order to another will take place over a broader range of chloride concentrations.

The experimental OER and CER reaction orders can be approximated from the derivative of log–log plots (see Figures S 15 and S 16) of the i vs $[Cl^-]$ curves. The results are shown in Figure 7. We previously performed RRDE studies similar to those described in this report using amorphous IrO$_x$.[38] The reaction orders for OER and CER obtained in those studies have been included for comparison. We want to note that for all values of $[Cl^-] < 10$ mM in Figure 7, the results may not be fully reliable due to possible interference of oxide formation on the Pt ring used for detection.[38]

We will first focus our discussion of the OER reaction order to $[Cl^-]$ concentrations of up to 50 mM (see Figure S 17 for a close-up of this region). In this range, $\mathcal{R}_{Cl^-}^{OER}$ has a negative fractional value between -0.2 and -0.4 for all materials tested in this study, as was already apparent from the continuous decrease in OER activity in Figure 6A. Interestingly, the previously characterized IrO$_x$ has a value of $\mathcal{R}_{Cl^-}^{OER}$ closest to 0, varying between 0 and -0.1. This is illustrative of this material's OER kinetics being almost impervious to the presence of chloride or parallel chlorine evolution, in contrast with the materials in the present study. For the double perovskites, $\mathcal{R}_{Cl^-}^{OER}$ is generally less negative the higher the intrinsic activity of the material, except for the IrO$_2$ reference, which shows relatively low activity but globally also one of the least negative values of $\mathcal{R}_{Cl^-}^{OER}$. Furthermore, most OER Tafel curves exhibit negligible changes in slope after the addition of Cl$^-$, except for Ba$_2$CeIrO$_6$ (see Figure S 11 for a comparison and Table S 3 for the full data). This suggests that Cl$^-$ does not change the OER mechanism, which (along with the decreasing fractional reaction order in Figure 6A) is in agreement with the simple site blocking model. However, the extent of blocking appears to depend sensitively on the type of material. We hypothesize that site blocking for a more amorphous catalyst is different from that in a less amorphous system. The OER data at $[Cl^-]$ exceeding 50 mM are subject to increasing levels of uncertainty, due to inherent limitations of the experiment; with rising chloride concentration, the CER contribution starts to dominate the OER current as a result of which the experimental noise is greatly amplified in subtle slope changes of the log–log plots. Extensive averaging or smoothing may alleviate the noise, but we chose to present the data as-is to illustrate limitations of the method. Despite the noise, the overall trend nonetheless suggests that the reaction order never reaches -1 but rather seems to increase again to sometimes even positive values. This may reflect the influence of chloride on the actual structure of the catalytic interface.

Regarding the CER in Figure 7B, $\mathcal{R}_{Cl^-}^{CER}$ also decreases continuously for all double perovskites, down to values of roughly 0.5, but for IrO$_2$, it stays at a constant value close to unity, $\mathcal{R}_{Cl^-}^{CER} \approx 0.92$. The IrO$_x$ reference material shows even different values, with $\mathcal{R}_{Cl^-}^{CER} \approx 1.45$ around $[Cl^-] = 10$ mM, which then progressively decreases to a steady value of 1.07. A $\mathcal{R}_{Cl^-}^{CER}$ value close to one has often been reported on metal oxides.[13,25,73,79,80] Furthermore, a decrease in $\mathcal{R}_{Cl^-}^{CER}$ as a result of an increase in $[Cl^-]$ has been reported previously on RuO$_2$.[81] Judging from reaction orders alone, it thus seems likely that both IrO$_x$ and IrO$_2$ follow a Volmer–Heyrovský mechanism, as their reaction orders converge near 1 at higher $[Cl^-]$. This is in agreement with previous reports.[13] On the other hand, reaction orders on all double perovskites continuously decrease to values much lower than 1. Such behavior is more expected of either a Volmer–Tafel or Volmer–Krishtalik mechanism dominating the kinetics. We further investigated the CER mechanism using methods devised by Conway et al.[82] and Ferro et al.[83] By reordering the measured CER i–E curves, one can test whether a Volmer–Tafel or Volme-–Heyrovský mechanism applies (see Figure S 13 and its description for details about the method). For IrO$_2$, we obtained a straight line in a Ferro–de Battisti test plot only, indicating Volmer–Heyrovský kinetics. We note that a straight line in such a plot can also indicate Volmer–Krishtalik kinetics; however, the y-intercept is then expected to be independent of $[Cl^-]$. Instead, the intercept shows an inverse $[Cl^-]$ dependence, which matches well with the V–H pathway (see Figure S 14 for more details). On the other hand, Ba$_2$PrIrO$_6$ only showed a straight line in a Conway–Novak test plot, suggesting that CER proceeds via a Volmer–Tafel mechanism on this material (and perhaps also on the other perovskites), in agreement with the reaction order findings.

As a final note, it can be expected that the apparent OER and CER chloride reaction orders on the double perovskites are affected by adventitious surface leaching as described in section 3.1. This leaching should lead to transient changes of the active surface area, and its effect on either $\mathcal{R}_{Cl^-}^{OER}$ or $\mathcal{R}_{Cl^-}^{CER}$ can be modeled via

$$i = A([Cl^-])j \tag{18}$$

where i is the measured current for either OER or CER, j is the current density as modeled by either the V–T or V–H model, and A is the real electrochemical surface area, which is dependent on chloride concentration due to leaching. It then follows that

$$\mathcal{R}_{Cl^-} = \left(\frac{\partial \ln i}{\partial \ln[Cl^-]}\right)_E = \frac{\partial \ln j}{\partial \ln[Cl^-]} + \frac{\partial \ln A([Cl^-])}{\partial \ln[Cl^-]} \tag{19}$$

On the right-hand side, the first term corresponds to the "kinetic" reaction order, as discussed earlier in this section. The second term represents the influence of chloride on the real surface area. As seen in Figure 1 and Table S2, the leaching rates of both noble and non-noble components are chloride-dependent but not in the same manner; a complex interplay can be expected from surface area changes due to increasing chloride concentration. Not much is currently known on the growth of amorphous surface phases on these materials in acidic media, meaning that the value and range of the A term is not easy to quantify. A reasonable assumption is that the term $\frac{\partial \ln A([\mathrm{Cl}^-])}{\partial \ln[\mathrm{Cl}^-]}$ is positive immediately upon contacting the pristine perovskite with acidic electrolyte, during which the majority of surface leaching takes place and the change in surface area should be the largest. Considering that the rate of leaching steadily decreases over time in Figure 1, we may expect A to approach a constant value for all values of $[\mathrm{Cl}^-]$, and its contribution to the reaction order should then tend to 0. On the other hand, if the rate of leaching increases strongly with increasing $[\mathrm{Cl}^-]$, increasing changes of A could explain the apparent rise in reaction orders for both OER and CER at higher $[\mathrm{Cl}^-]$ concentrations.

4. CONCLUSIONS

In this work, we report that iridium-based double perovskites with structures Ba_2BIrO_6 (B = Pr, Nd, La, Sn, Y, Tb, Ce) and Sr_2YIrO_6, previously reported having high oxygen evolution activity in acidic media, also show high catalytic activity toward chlorine evolution in relatively low chloride concentrations (0−120 mM). A strong linear correlation between CER and OER activity was found on all catalysts employed and also comparable selectivity. This strengthens the suggestion that OER and CER follow a scaling relationship, as suggested in previous studies. On the basis of these results, we expect that promoting one reaction over the other on the basis of kinetic considerations alone may be exceedingly difficult, if not impossible. Alternative pathways, such as affecting the CER thermodynamics through pH changes or the mass transport of chloride to the active catalyst, are likely more successful in enhancing selectivity.[24] Electrochemical ICP-MS measurements showed that chloride has mixed effects on the stability of the perovskites, whereas non-noble dissolution effects were inconclusive; it significantly enhanced iridium dissolution during potentiodynamic control and active OER/CER, as evidenced by a lower value of the S-number. Dissolution pathways related to OER and CER are therefore likely different, which must be taken into account when considering an active catalyst for either of the reactions. Reaction order analysis indicates that CER proceeds via the Volmer−Tafel mechanism on the double perovskites, whereas it follows a Volmer−Heyrovský mechanism on IrO_2 and amorphous IrO_x. Contrary to amorphous IrO_x, the OER activity on the double perovskites and IrO_2 is strongly impacted by chloride concentration, displaying fractional, negative reaction orders.

■ ASSOCIATED CONTENT

Ⓢ Supporting Information

The Supporting Information is available free of charge on the ACS Publications website at DOI: 10.1021/acscatal.9b01159.

> Supplementary ICP-MS data and methodology description, XRD data, RRDE data concerning voltammetric characterizations, estimation of errors concerning RRDE chlorine detection, effect of Nafion on CER selectivity, ECSA determination and error bars, numerical Tafel slope values, OER vs CER selectivity, and test plots for the CER mechanism (PDF)

■ AUTHOR INFORMATION

Corresponding Author

*E-mail: m.koper@chem.leidenuniv.nl.

ORCID ⓘ

Nickson Perini: 0000-0002-3319-5102

Serhiy Cherevko: 0000-0002-7188-4857

Marc T. M. Koper: 0000-0001-6777-4594

Notes

The authors declare no competing financial interest.

■ REFERENCES

(1) Carmo, M.; Fritz, D. L.; Mergel, J.; Stolten, D. A Comprehensive Review on PEM Water Electrolysis. *Int. J. Hydrogen Energy* **2013**, *38*, 4901−4934.

(2) Lakshmanan, S.; Murugesan, T. The Chlor-Alkali Process: Work in Progress. *Clean Technol. Environ. Policy* **2014**, *16*, 225−234.

(3) Crook, J.; Mousavi, A. The Chlor-Alkali Process: A Review of History and Pollution. *Environ. Forensics* **2016**, *17*, 211−217.

(4) Lewis, N. S. Toward Cost-Effective Solar Energy Use. *Science* **2007**, *315*, 798−801.

(5) Katsounaros, I.; Cherevko, S.; Zeradjanin, A. R.; Mayrhofer, K. J. J. Oxygen Electrochemistry as a Cornerstone for Sustainable Energy Conversion. *Angew. Chem., Int. Ed.* **2014**, *53*, 102−121.

(6) Fauvarque, J. The Chlorine Industry. *Pure Appl. Chem.* **1996**, *68*, 1713−1720.

(7) Euro Chlor. *Chlor-alkali Industry Review 2017/2018, Manufacturing & Applications*, https://chlorineindustryreview.com/manufacturing-applications/ (accessed on November 28, 2018).

(8) Koper, M. T. M. Thermodynamic Theory of Multi-Electron Transfer Reactions: Implications for Electrocatalysis. *J. Electroanal. Chem.* **2011**, *660*, 254−260.

(9) Trasatti, S. Electrocatalysis: Understanding the Success of DSA®. *Electrochim. Acta* **2000**, *45*, 2377−2385.

(10) Moussallem, I.; Jörissen, J.; Kunz, U.; Pinnow, S.; Turek, T. Chlor-Alkali Electrolysis with Oxygen Depolarized Cathodes: History, Present Status and Future Prospects. *J. Appl. Electrochem.* **2008**, *38*, 1177−1194.

(11) Jung, J.; Postels, S.; Bardow, A. Cleaner Chlorine Production Using Oxygen Depolarized Cathodes? A Life Cycle Assessment. *J. Cleaner Prod.* **2014**, *80*, 46−56.

(12) Wang, X.; Tong, C.; Palazoglu, A.; El-Farra, N. H. Energy Management for the Chlor-Alkali Process with Hybrid Renewable Energy Generation Using Receding Horizon Optimization. In *53rd IEEE Conference on Decision and Control*, Los Angeles, CA, December 15−17, 2014; pp 4838−4843.

(13) Trasatti, S. Progress in the Understanding of the Mechanism of Chlorine Evolution at Oxide Electrodes. *Electrochim. Acta* **1987**, *32*, 369−382.

(14) Duby, P. The History of Progress in Dimensionally Stable Anodes. *JOM* **1993**, *45*, 41−43.

(15) Karlsson, R. K. B.; Cornell, A. Selectivity between Oxygen and Chlorine Evolution in the Chlor-Alkali and Chlorate Processes. *Chem. Rev.* **2016**, *116*, 2982−3028.

(16) Jefferson, M. A Renewable Energy Future? In *Handbook on Energy and Climate Change*; Edward Elgar Publishing, 2013; Vol. *285*, pp 254−269.

(17) Zeng, K.; Zhang, D. Recent Progress in Alkaline Water Electrolysis for Hydrogen Production and Applications. *Prog. Energy Combust. Sci.* **2010**, *36*, 307−326.

(18) Man, I. C.; Su, H. Y.; Calle-Vallejo, F.; Hansen, H. A.; Martínez, J. I.; Inoglu, N. G.; Kitchin, J.; Jaramillo, T. F.; Nørskov, J. K.; Rossmeisl, J. Universality in Oxygen Evolution Electrocatalysis on Oxide Surfaces. *ChemCatChem* **2011**, *3*, 1159−1165.

(19) Fabbri, E.; Schmidt, T. J. Oxygen Evolution Reaction—The Enigma in Water Electrolysis. *ACS Catal.* **2018**, *8*, 9765−9774.

(20) Panić, V. V.; Dekanski, A. B.; Milonjić, S. K.; Mišković-Stanković, V. B.; Nikolić, B. Ž. Electrocatalytic Activity of Sol-Gel-Prepared RuO2/Ti Anode in Chlorine and Oxygen Evolution Reactions. *Russ. J. Electrochem.* **2006**, *42*, 1055−1060.

(21) Hoseinieh, S. M.; Ashrafizadeh, F.; Maddahi, M. H. A Comparative Investigation of the Corrosion Behavior of RuO[Sub 2]−IrO[Sub 2]−TiO[Sub 2] Coated Titanium Anodes in Chloride Solutions. *J. Electrochem. Soc.* **2010**, *157*, E50.

(22) Shao, D.; Yan, W.; Cao, L.; Li, X.; Xu, H. High-Performance Ti/Sb−SnO2/Pb3O4 Electrodes for Chlorine Evolution: Preparation and Characteristics. *J. Hazard. Mater.* **2014**, *267*, 238−244.

(23) Fujimura, K.; Izumiya, K.; Kawashima, A.; Akiyama, E.; Habazaki, H.; Kumagai, N.; Hashimoto, K. Anodically Deposited Manganese-Molybdenum Oxide Anodes with High Selectivity for Evolving Oxygen in Electrolysis of Seawater. *J. Appl. Electrochem.* **1999**, *29*, 769−775.

(24) Vos, J. G.; Wezendonk, T. A.; Jeremiasse, A. W.; Koper, M. T. M. MnOx/IrOx as Selective Oxygen Evolution Electrocatalyst in Acidic Chloride Solution. *J. Am. Chem. Soc.* **2018**, *140*, 10270−10281.

(25) Trasatti, S. Electrocatalysis in the Anodic Evolution of Oxygen and Chlorine. *Electrochim. Acta* **1984**, *29*, 1503−1512.

(26) Hansen, H. A.; Man, I. C.; Studt, F.; Abild-Pedersen, F.; Bligaard, T.; Rossmeisl, J. Electrochemical Chlorine Evolution at Rutile Oxide (110) Surfaces. *Phys. Chem. Chem. Phys.* **2010**, *12*, 283−290.

(27) Abbott, D. F.; Petrykin, V.; Okube, M.; Bastl, Z.; Mukerjee, S.; Krtil, P. Selective Chlorine Evolution Catalysts Based on Mg-Doped Nanoparticulate Ruthenium Dioxide. *J. Electrochem. Soc.* **2015**, *162*, H23−H31.

(28) Exner, K. S.; Anton, J.; Jacob, T.; Over, H. Controlling Selectivity in the Chlorine Evolution Reaction over RuO2 -Based Catalysts. *Angew. Chem., Int. Ed.* **2014**, *53*, 11032−11035.

(29) Exner, K. S.; Anton, J.; Jacob, T.; Over, H. Full Kinetics from First Principles of the Chlorine Evolution Reaction over a RuO2 (110) Model Electrode. *Angew. Chem., Int. Ed.* **2016**, *55*, 7501−7504.

(30) Sohrabnejad-Eskan, I.; Goryachev, A.; Exner, K. S.; Kibler, L. A.; Hensen, E. J. M.; Hofmann, J. P.; Over, H. Temperature-Dependent Kinetic Studies of the Chlorine Evolution Reaction over RuO2 (110) Model Electrodes. *ACS Catal.* **2017**, *7*, 2403−2411.

(31) Lassali, T. A. F.; Boodts, J. F. C.; Trasatti, S. Electrocatalytic Activity of the Ternary Oxide Ru0.3PtxTi(0.7 — x)O2 for Chlorine Evolution. *Electrochim. Acta* **1994**, *39*, 1545−1549.

(32) Macounová, K. M.; Makarova, M.; Jirkovský, J. S.; Franc, J.; Krtil, P. Parallel Oxygen and Chlorine Evolution on Ru1−xNixO2−y Nanostructured Electrodes. *Electrochim. Acta* **2008**, *53*, 6126−6134.

(33) Petrykin, V.; Macounová, K. M.; Okube, M.; Mukerjee, S.; Krtil, P. Local Structure of Co Doped RuO2 Nanocrystalline Electrocatalytic Materials for Chlorine and Oxygen Evolution. *Catal. Today* **2013**, *202*, 63−69.

(34) Consonni, V.; Trasatti, S.; Pollak, F. H.; O'Grady, W. E. Mechanism of Chlorine Evolution on Oxide Anodes: Study of PH Effects. *J. Electroanal. Chem. Interfacial Electrochem.* **1987**, *228*, 393−406.

(35) Spöri, C.; Kwan, J. T. H.; Bonakdarpour, A.; Wilkinson, D. P.; Strasser, P. The Stability Challenges of Oxygen Evolving Catalysts:

(36) Diaz-Morales, O.; Raaijman, S.; Kortlever, R.; Kooyman, P. J.; Wezendonk, T.; Gascon, J.; Fu, W. T.; Koper, M. T. M. Iridium-Based Double Perovskites for Efficient Water Oxidation in Acid Media. *Nat. Commun.* **2016**, *7*, 12363.

(37) Geiger, S.; Kasian, O.; Ledendecker, M.; Pizzutilo, E.; Mingers, A. M.; Fu, W. T.; Diaz-Morales, O.; Li, Z.; Oellers, T.; Fruchter, L.; Ludwig, A.; Mayrhofer, K. J. J.; Koper, M. T. M.; Cherevko, S. The Stability Number as a Metric for Electrocatalyst Stability Benchmarking. *Nat. Catal.* **2018**, *1*, 508−515.

(38) Vos, J. G.; Koper, M. T. M. Measurement of Competition between Oxygen Evolution and Chlorine Evolution Using Rotating Ring-Disk Electrode Voltammetry. *J. Electroanal. Chem.* **2018**, *819*, 260−268.

(39) Fu, W. T.; IJdo, D. J. W. On the Space Group of the Double Perovskite Ba2PrIrO6. *J. Solid State Chem.* **2005**, *178*, 1312−1316.

(40) Fu, W. T.; IJdo, D. J. W. Re-Examination of the Structure of Ba2MIrO6 (M = La, Y): Space Group Revised. *J. Alloys Compd.* **2005**, *394*, L5.

(41) Schuppert, A. K.; Topalov, A. A.; Katsounaros, I.; Klemm, S. O.; Mayrhofer, K. J. J. A Scanning Flow Cell System for Fully Automated Screening of Electrocatalyst Materials. *J. Electrochem. Soc.* **2012**, *159*, F670−F675.

(42) Klemm, S. O.; Topalov, A. A.; Laska, C. A.; Mayrhofer, K. J. J. Coupling of a High Throughput Microelectrochemical Cell with Online Multielemental Trace Analysis by ICP-MS. *Electrochem. Commun.* **2011**, *13*, 1533−1535.

(43) Kasian, O.; Geiger, S.; Mayrhofer, K. J. J.; Cherevko, S. Electrochemical On-Line ICP-MS in Electrocatalysis Research. *Chem. Rec.* **2018**, DOI: 10.1002/tcr.201800162.

(44) Gileadi, E. Problems in Interfacial Electrochemistry That Have Been Swept under the Carpet. *J. Solid State Electrochem.* **2011**, *15*, 1359−1371.

(45) Vesztergom, S.; Ujvári, M.; Láng, G. G. Dual Cyclic Voltammetry with Rotating Ring−Disk Electrodes. *Electrochim. Acta* **2013**, *110*, 49−55.

(46) Vesztergom, S.; Barankai, N.; Kovács, N.; Ujvári, M.; Siegenthaler, H.; Broekmann, P.; Láng, G. G. Electrical Cross-Talk in Four-Electrode Experiments. *J. Solid State Electrochem.* **2016**, *20*, 3165−3177.

(47) McCrory, C. C. L.; Jung, S.; Peters, J. C.; Jaramillo, T. F. Benchmarking Heterogeneous Electrocatalysts for the Oxygen Evolution Reaction. *J. Am. Chem. Soc.* **2013**, *135*, 16977−16987.

(48) Seitz, L. C.; Dickens, C. F.; Nishio, K.; Hikita, Y.; Montoya, J.; Doyle, A.; Kirk, C.; Vojvodic, A.; Hwang, H. Y.; Norskov, J. K.; Jaramillo, T. F. A Highly Active and Stable IrOx /SrIrO3 Catalyst for the Oxygen Evolution Reaction. *Science (Washington, DC, U. S.)* **2016**, *353*, 1011−1014.

(49) Topalov, A. A.; Katsounaros, I.; Auinger, M.; Cherevko, S.; Meier, J. C.; Klemm, S. O.; Mayrhofer, K. J. J. Dissolution of Platinum: Limits for the Deployment of Electrochemical Energy Conversion? *Angew. Chem., Int. Ed.* **2012**, *51*, 12613−12615.

(50) Geiger, S.; Cherevko, S.; Mayrhofer, K. J. J. Dissolution of Platinum in Presence of Chloride Traces. *Electrochim. Acta* **2015**, *179*, 24−31.

(51) Kasian, O.; Grote, J.-P.; Geiger, S.; Cherevko, S.; Mayrhofer, K. J. J. The Common Intermediates of Oxygen Evolution and Dissolution Reactions during Water Electrolysis on Iridium. *Angew. Chem., Int. Ed.* **2018**, *57*, 2488−2491.

(52) Wakeshima, M.; Harada, D.; Hinatsu, Y. Crystal Structures and Magnetic Properties of Ordered Perovskites Ba2LnIrO6 (Ln = Lanthanide). *J. Mater. Chem.* **2000**, *10*, 419−422.

(53) Massué, C.; Huang, X.; Tarasov, A.; Ranjan, C.; Cap, S.; Schlögl, R. Microwave Assisted Synthesis of Stable and Highly Active Ir-Oxohydroxides for Electrochemical Oxidation of Water. *ChemSusChem* **2017**, *10*, 1958.

(54) Zaharieva, I.; Chernev, P.; Risch, M.; Klingan, K.; Kohlhoff, M.; Fischer, A.; Dau, H. Electrosynthesis, Functional, and Structural

Characterization of a Water-Oxidizing Manganese Oxide. *Energy Environ. Sci.* **2012**, *5*, 7081−7089.

(55) Balaji, R.; Kannan, B. S.; Lakshmi, J.; Senthil, N.; Vasudevan, S.; Sozhan, G.; Shukla, A. K.; Ravichandran, S. An Alternative Approach to Selective Sea Water Oxidation for Hydrogen Production. *Electrochem. Commun.* **2009**, *11*, 1700−1702.

(56) Mo, Y.; Stefan, I. C.; Cai, W.-B.; Dong, J.; Carey, P.; Scherson, D. A. In Situ Iridium L III -Edge X-Ray Absorption and Surface Enhanced Raman Spectroscopy of Electrodeposited Iridium Oxide Films in Aqueous Electrolytes. *J. Phys. Chem. B* **2002**, *106*, 3681−3686.

(57) Sanchez Casalongue, H. G.; Ng, M. L.; Kaya, S.; Friebel, D.; Ogasawara, H.; Nilsson, A. In Situ Observation of Surface Species on Iridium Oxide Nanoparticles during the Oxygen Evolution Reaction. *Angew. Chem., Int. Ed.* **2014**, *53*, 7169−7172.

(58) Minguzzi, A.; Lugaresi, O.; Achilli, E.; Locatelli, C.; Vertova, A.; Ghigna, P.; Rondinini, S. Observing the Oxidation State Turnover in Heterogeneous Iridium-Based Water Oxidation Catalysts. *Chem. Sci.* **2014**, *5*, 3591.

(59) Pfeifer, V.; Jones, T. E.; Velasco Vélez, J. J.; Massué, C.; Arrigo, R.; Teschner, D.; Girgsdies, F.; Scherzer, M.; Greiner, M. T.; Allan, J.; Hashagen, M.; Weinberg, G.; Piccinin, S.; Hävecker, M.; Knop-Gericke, A.; Schlögl, R. The Electronic Structure of Iridium and Its Oxides. *Surf. Interface Anal.* **2016**, *48*, 261−273.

(60) Massué, C.; Pfeifer, V.; van Gastel, M.; Noack, J.; Algara-Siller, G.; Cap, S.; Schlögl, R. Reactive Electrophilic O I− Species Evidenced in High-Performance Iridium Oxohydroxide Water Oxidation Electrocatalysts. *ChemSusChem* **2017**, *10*, 4786−4798.

(61) Kuznetsova, E.; Petrykin, V.; Sunde, S.; Krtil, P. Selectivity of Nanocrystalline IrO2-Based Catalysts in Parallel Chlorine and Oxygen Evolution. *Electrocatalysis* **2015**, *6*, 198−210.

(62) Cherevko, S.; Geiger, S.; Kasian, O.; Kulyk, N.; Grote, J.-P.; Savan, A.; Shrestha, B. R.; Merzlikin, S.; Breitbach, B.; Ludwig, A.; Mayrhofer, K. J. J. Oxygen and Hydrogen Evolution Reactions on Ru, RuO2, Ir, and IrO2 Thin Film Electrodes in Acidic and Alkaline Electrolytes: A Comparative Study on Activity and Stability. *Catal. Today* **2016**, *262*, 170−180.

(63) Stevens, M. B.; Enman, L. J.; Batchellor, A. S.; Cosby, M. R.; Vise, A. E.; Trang, C. D. M.; Boettcher, S. W. Measurement Techniques for the Study of Thin Film Heterogeneous Water Oxidation Electrocatalysts. *Chem. Mater.* **2017**, *29*, 120−140.

(64) Watzele, S.; Bandarenka, A. S. Quick Determination of Electroactive Surface Area of Some Oxide Electrode Materials. *Electroanalysis* **2016**, *28*, 2394−2399.

(65) Chow, K. F.; Carducci, T. M.; Murray, R. W. Electronic Conductivity of Films of Electroflocculated 2 Nm Iridium Oxide Nanoparticles. *J. Am. Chem. Soc.* **2014**, *136*, 3385−3387.

(66) Jung, S.; McCrory, C. C. L.; Ferrer, I. M.; Peters, J. C.; Jaramillo, T. F. Benchmarking Nanoparticulate Metal Oxide Electrocatalysts for the Alkaline Water Oxidation Reaction. *J. Mater. Chem. A* **2016**, *4*, 3068−3076.

(67) Batchellor, A. S.; Boettcher, S. W. Pulse-Electrodeposited Ni−Fe (Oxy)Hydroxide Oxygen Evolution Electrocatalysts with High Geometric and Intrinsic Activities at Large Mass Loadings. *ACS Catal.* **2015**, *5*, 6680−6689.

(68) Takeno, N. *Atlas of Eh-pH Diagrams Intercomparison of Thermodynamic Databases*, Geological Survey of Japan Open File Report No. 419, National Institute of Advanced Industrial Science and Technology Research Center for Deep Geological Environments, 2005.

(69) Zou, X.; Liu, Y.; Li, G.-D.; Wu, Y.; Liu, D.-P.; Li, W.; Li, H.-W.; Wang, D.; Zhang, Y.; Zou, X. Ultrafast Formation of Amorphous Bimetallic Hydroxide Films on 3D Conductive Sulfide Nanoarrays for Large-Current-Density Oxygen Evolution Electrocatalysis. *Adv. Mater.* **2017**, *29*, 1700404.

(70) Pi, Y.; Shao, Q.; Wang, P.; Lv, F.; Guo, S.; Guo, J.; Huang, X. Trimetallic Oxyhydroxide Coralloids for Efficient Oxygen Evolution Electrocatalysis. *Angew. Chem., Int. Ed.* **2017**, *56*, 4502−4506.

(71) Nai, J.; Lu, Y.; Yu, L.; Wang, X.; Lou, X. W. D. Formation of Ni-Fe Mixed Diselenide Nanocages as a Superior Oxygen Evolution Electrocatalyst. *Adv. Mater.* **2017**, *29*, 1703870.

(72) Guerrini, E.; Trasatti, S. Recent Developments in Understanding Factors of Electrocatalysis. *Russ. J. Electrochem.* **2006**, *42*, 1017−1025.

(73) Tilak, B. V.; Conway, B. E. Analytical Relations between Reaction Order and Tafel Slope Derivatives for Electrocatalytic Reactions Involving Chemisorbed Intermediates. *Electrochim. Acta* **1992**, *37*, 51−63.

(74) Rosestolato, D.; Fregoni, J.; Ferro, S.; De Battisti, A. Influence of the Nature of the Electrode Material and Process Variables on the Kinetics of the Chlorine Evolution Reaction. The Case of IrO2-Based Electrocatalysts. *Electrochim. Acta* **2014**, *139*, 180−189.

(75) Krishtalik, L. I. Kinetics and Mechanism of Anodic Chlorine and Oxygen Evolution Reactions on Transition Metal Oxide Electrodes. *Electrochim. Acta* **1981**, *26*, 329−337.

(76) Exner, K. S.; Anton, J.; Jacob, T.; Over, H. Chlorine Evolution Reaction on RuO2(110): Ab Initio Atomistic Thermodynamics Study - Pourbaix Diagrams. *Electrochim. Acta* **2014**, *120*, 460−466.

(77) Koper, M. T. M. A Lattice-Gas Model for Halide Adsorption on Single-Crystal Electrodes. *J. Electroanal. Chem.* **1998**, *450*, 189−201.

(78) Fernández, J. L.; Gennero de Chialvo, M. R.; Chialvo, A. C. Kinetic Study of the Chlorine Electrode Reaction on Ti/RuO2 through the Polarisation Resistance. *Electrochim. Acta* **2002**, *47*, 1137−1144.

(79) Santana, M. H. P.; De Faria, L. A. Oxygen and Chlorine Evolution on RuO2+TiO2+CeO2+Nb2O5Mixed Oxide Electrodes. *Electrochim. Acta* **2006**, *51*, 3578−3585.

(80) Boggio, R.; Carugati, A.; Lodi, G.; Trasatti, S. Mechanistic Study of Cl2 Evolution at Ti-Supported Co3O4 Anodes. *J. Appl. Electrochem.* **1985**, *15*, 335−349.

(81) Conway, B. E.; Ping, G.; De Battisti, A.; Barbieri, A.; Battaglin, G. Behaviour of the Adsorbed Cl* Intermediate in Anodic Cl2 Evolution at Thin-Film RuO2 Surfaces. *J. Mater. Chem.* **1991**, *1*, 725.

(82) Conway, B. E.; Novak, D. M. Chloride Ion Adsorption Effects in the Recombination-Controlled Kinetics of Anodic Chlorine Evolution at Pt Electrodes. *J. Chem. Soc., Faraday Trans. 1* **1979**, *75*, 2454−2472.

(83) Ferro, S.; De Battisti, A. Electrocatalysis and Chlorine Evolution Reaction at Ruthenium Dioxide Deposited on Conductive Diamond. *J. Phys. Chem. B* **2002**, *106*, 2249−2254.